

Self-Healing of Surfactant Surface Micelles on Millisecond Time Scales

Hannes C. Schniepp, Dudley A. Saville, and Ilhan A. Aksay*

Department of Chemical Engineering, Princeton University, Princeton, New Jersey 08544

Received April 10, 2006; Revised Manuscript Received August 21, 2006; E-mail: iaksay@princeton.edu

Micellar coatings of surfactants at solid–liquid interfaces can provide colloidal stability,^{1,2} corrosion inhibition,³ and boundary lubrication.^{4–6} Understanding the dynamics of such coatings is necessary to the optimization of self-healing, a characteristic of micellar structures. Self-healing rates that are sufficient to counter the rate of defect formation due to physical or chemical attack are required for successful engineering applications. Although some dynamic parameters of bulk and surface processes have been reported,^{7–10} the time scale for micellar surface self-assembly remains unknown. In this work, we present a novel atomic force microscopy (AFM) technique that allows us to visualize this self-healing process over millisecond time scales at nanometer spatial resolution. No traditional technique used to detect surface adlayers, including neutron reflectometry,¹¹ optical reflectometry,^{12,13} ellipsometry,¹⁴ and Fourier transform infrared spectroscopy (FTIR)¹⁰ combines such high temporal and spatial resolutions. Using our new method, we show that nanometer-sized defects in a crystalline array of surface micelles recover flawlessly in less than ~ 6 ms.

The highly ordered, self-assembled micellar structures formed by surfactants at the solid–liquid interface were first revealed by AFM.^{15–17} Depending on the surfactant/surface combination, different morphologies such as full or half spherical and cylindrical micelles were found, often organized into large crystalline arrays of surface micelles. Since typical AFM acquisition times are on the order of minutes, these studies treated such aggregates as seemingly static, neglecting their dynamic behavior¹⁸ at different time scales. While the lateral diffusion rates of individual surfactants within flat surfactant layers are known,^{19,20} the actual aggregation of molecules into micelles and their organization into micellar crystals are potentially much slower.²¹ Similarly, in bulk surfactant solutions the exchange time of surfactant monomers between micellar aggregates and the solvent, $\tau_{1,\text{bulk}}$ (micro- to milliseconds) is much faster than the formation time of an entire micelle from individual molecules and the corresponding disintegration time, $\tau_{2,\text{bulk}}$ (milliseconds).^{7–9} Using AFM force-displacement curves at different approach frequencies, Clark and Ducker suggested that the reorganization of surfactants on a silica surface may occur within times as short as 20 ms.¹⁰ However, since the force-displacement method does not provide images, it is impossible to know if the micellar film was punctured or only compressed. Thus, their results cannot be used to draw definite conclusions on how fast surfactants self-assemble into micellar arrays on surfaces. With our technique, the AFM tip demonstrably pierces the surfactant adlayer, thereby imaging the lattice of the underlying substrate (Figure 1). Using the same tip, we simultaneously image the micellar structure of the adlayer on the substrate and thus are able to immediately monitor the adlayer's response to the tip-induced defect (Figure 1).

In previous AFM imaging studies of surfactant surface aggregates, very low force set points were used to keep the tip above the very weakly bound aggregate layer through repulsive forces in the electric double-layer.²² Figure 1a shows the crystalline array

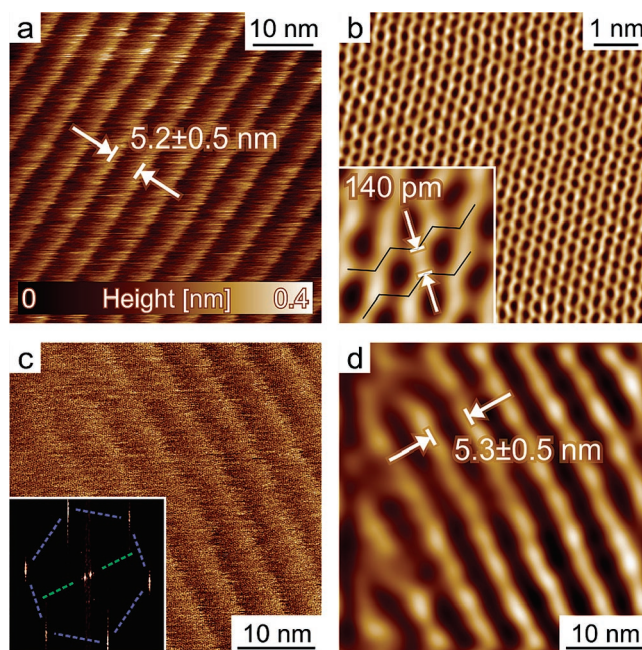


Figure 1. AFM images of surfactant aggregates on graphite: (a) low-force topography image; (b) small, high-force friction image, showing the graphite lattice only; (c) larger, high-force friction image, showing aggregates and lattice simultaneously; (inset) Fourier transform. The blue and green lines highlight the orientation of lattice and micelles, respectively. Panel d shows a band-pass filtered version of panel c.

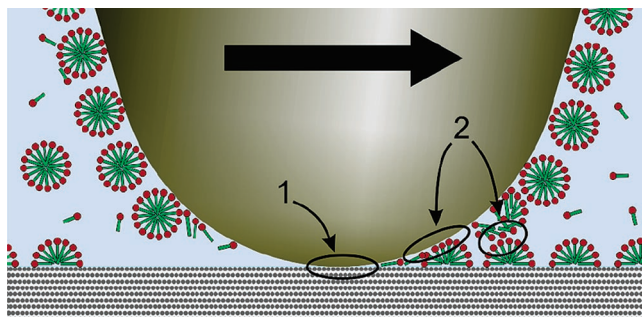


Figure 2. Schematic of AFM tip at high force, simultaneously touching both the substrate at contact area “1” and the micellar aggregates at potential contact areas “2”.

of hemicylindrical surface micelles that is detected under these conditions at the interface of highly oriented pyrolytic graphite (HOPG) and a 10 mM solution of sodium dodecyl sulfate (SDS). If the force is then increased by just a few hundred pN, the probe overwhelms the repulsive force, pierces the surfactant layer and makes contact with the substrate, as illustrated in Figure 2. In this case, the substrate rather than the adsorbate is imaged.

Our new imaging technique purposely operates in this high-force regime. In addition to acquiring the deflection and topography signals as in previous work, we also monitor the cantilever torsion

which represents the friction between tip and sample. As expected, this friction signal reveals the honeycomb lattice of the graphite substrate, without any apparent signal from the surfactant aggregates, shown in Figure 1b. When larger areas are scanned under otherwise identical parameters, the friction images not only show the lattice, but—surprisingly—the signature of the micellar aggregates simultaneously, visible in Figure 1c in the shape of diagonal stripes. At the reduced magnification necessary to reveal this micellar signal, the much smaller graphite lattice is very hard to recognize in what appears to be background “noise”. It is, however, easily revealed by the Fourier transform of Figure 1c, displayed as an inset to Figure 1c, conveniently demonstrating the simultaneous imaging of micelles and lattice at two significantly different length scales: the stripes in Figure 1c, produced by the hemicylindrical micelles, translate into two dots close to the center of the transform; the honeycomb lattice of graphite is represented by the hexagonal pattern at much higher spatial frequencies. The blue and green lines superimposed on the inset image highlight the orientation of the substrate lattice and the micellar array, respectively, confirming that the surfactant structures are, within the precision of our technique, oriented perpendicular with a symmetry axis of the HOPG lattice, as expected.¹⁸ Application of a band-pass filter to Figure 1c increases the visibility of the stripes (Figure 1d) and allows us to determine the stripe periodicity as 5.3 ± 0.5 nm, in excellent agreement with the results of the traditional low-force imaging mode (Figure 1a).

We explain the imaging behavior by referring to the simplified schematic in Figure 2. The observation that all our high-force images show the substrate lattice with its 140 pm bond length proves that the AFM tip is in contact with the substrate in the region denoted by “1”, giving rise to the atomic-scale friction modulations. We estimate that the surfactant adlayer is completely displaced in a circular area of at least 9 nm in diameter (see Supporting Information). As the tip is moved toward the right, it contacts the surfactant layer in the areas denoted by “2” and ultimately strips these periodically adsorbed aggregates from the surface. It is thus not surprising that sliding the AFM probe across the surface at the described conditions exerts a torque on the cantilever that reflects the 5.3 nm periodicity of the adlayer, although we do not yet have a definite model to interpret this modulation, including the energetics of motion leading to the torque and the role of the hydrodynamics in the healing rates.

This imaging behavior also allows us to assess the temporal behavior of the surface aggregates. Since the spacing of two subsequent scan lines in Figure 1c is only 78 pm, the tip essentially samples the area from which aggregates had been removed during the preceding scan line—a stripe roughly 9 nm of width. Since the micellar surfactant pattern is still detected in every scan line, the tip-induced defects must recover within the time between two subsequent scan lines. These patterns stay identical in shape and modulation height when the line frequency is varied between 5 and 60 Hz. This shows that (i) recovery occurs in the time between two scan lines and that (ii) complete, flawless recovery of the crystalline array of hemicylindrical micelles is achieved, even at the highest line frequency of 60 Hz. Thorough analysis of the tip trajectory allows us to conclude that this recovery is complete within ~ 6 ms (see Supporting Information).

In bulk SDS solutions, where the transport-limited $\tau_{1,\text{bulk}}$ is ~ 20 μs , the formation of a bulk micelle takes as long as ~ 2 ms ($\tau_{2,\text{bulk}}$).⁸

On surfaces, the previously measured diffusion rates^{19,20} of 10^{-12} to 10^{-10} m^2/s would allow the closing of a 20 nm diameter hole within a few microseconds.²³ Similar to the bulk solution, we expect the self-assembly time of a surface micelle to be longer; our measurements show that the upper limit for this process is ~ 6 ms. On silica surfaces, adsorption and desorption times of surfactants are as long as seconds,¹⁰ which may indicate that the reorganization process described here is mainly because of redistribution of surfactant molecules on the surface rather than the exchange of the surfactants between the bulk liquid and the surface.

We have demonstrated that nanometer-scale defects in a crystalline array of surfactant surface micelles cure within 6 ms. Simultaneous imaging of both the substrate and the adsorbed layer of surfactant aggregates is achieved by monitoring friction forces while scanning in contact with the substrate. We thus acquire images at two “heights”, exhibiting features at the micellar and atomic length scales that are almost 2 orders of magnitude apart. We expect this technique to be of use not only in the study of the dynamic behavior of surfactant aggregates but with other adsorbed layers that exhibit a characteristic structural signature.

Acknowledgment. Financial support from the NASA University Research, Engineering, and Technology Institute on BioInspired Materials (BIMat) under Award No. NCC-1-02037 and from ARO/MURI under Grant No. W911NF-04-1-0170 is greatly appreciated.

Supporting Information Available: Information concerning the details of sample preparation, AFM imaging, tip geometry; and analysis of self-healing times. This material is available free of charge via the Internet at <http://pubs.acs.org>.

References

- (1) Subramanian, V.; Ducker, W. A. *J. Phys. Chem. B* **2001**, *105*, 1389–1402.
- (2) Russel, W. B.; Saville, D. A.; Schowalter, W. R. *Colloidal Dispersions*; Cambridge University Press: New York, 1989.
- (3) Wei, Z.; Somasundaran, P.; Duby, P. *J. Electrochem. Soc.* **2004**, *151*, B304–308.
- (4) Vakarelski, I. U.; Brown, S. C.; Rabinovich, Y. I.; Moudgil, B. M. *Langmuir* **2004**, *20*, 1724–1731.
- (5) Sulek, M. W.; Wasilewski, T. *Wear* **2006**, *260*, 193–204.
- (6) Hills, B. A. *Proc. Inst. Mech. Eng., Part H* **2000**, *214*, 83–94.
- (7) Mijnlieff, P. F.; Ditmarsch, R. *Nature* **1965**, *208*, 889–891.
- (8) Lang, J.; Tondre, C.; Zana, R. *J. Phys. Chem.* **1975**, *79*, 276–283.
- (9) Aniansson, E. A. G.; Wall, S. N.; Almgren, M.; Hoffmann, H.; Kielmann, I.; Ulbricht, W.; Zana, R.; Lang, J.; Tondre, C. *J. Phys. Chem.* **1976**, *80*, 905–922.
- (10) Clark, S. C.; Ducker, W. A. *J. Phys. Chem. B* **2003**, *107*, 9011–9021.
- (11) Fragneto, G.; Thomas, R. K.; Rennie, A. R.; Penfold, J. *Langmuir* **1996**, *12*, 6036–6043.
- (12) Pagac, E. S.; Prieve, D. C.; Tilton, R. D. *Langmuir* **1998**, *14*, 2333–2342.
- (13) Atkin, R.; Craig, V. S. J.; Biggs, S. *Langmuir* **2001**, *17*, 6155–6163.
- (14) Tiberg, F.; Jönsson, B.; Lindman, B. *Langmuir* **1994**, *10*, 3714–3722.
- (15) Manne, S.; Gaub, H. E. *Science* **1995**, *270*, 1480–1482.
- (16) Wanless, E. J.; Ducker, W. A. *J. Phys. Chem.* **1996**, *100*, 3207–3214.
- (17) Patrick, H. N.; Warr, G. G.; Manne, S.; Aksay, I. A. *Langmuir* **1997**, *13*, 4349–4356.
- (18) Saville, D. A.; Chun, J.; Li, J.-L.; Schniepp, H. C.; Car, R.; Aksay, I. A. *Phys. Rev. Lett.* **2006**, *96*, 018301.
- (19) Roberts, T. K. *Nature* **1973**, *242*, 348–348.
- (20) Berman, A. D.; Cameron, S. D.; Israelachvili, J. N. *J. Phys. Chem. B* **1997**, *101*, 5692–5697.
- (21) Yao, N.; Ku, A. Y.; Nakagawa, N.; Lee, T.; Saville, D. A.; Aksay, I. A. *Chem. Mater.* **2000**, *12*, 1536–1548.
- (22) Senden, T. J.; Drummond, C. J.; Kekicheff, P. *Langmuir* **1994**, *10*, 358–362.
- (23) The characteristic time, t , of this process is estimated by $t \approx (\text{characteristic length})^2/(\text{diffusivity})$, i.e., $(10 \text{ nm})^2/(10^{-11} \text{ m}^2/\text{s}) \approx 10 \mu\text{s}$.

JA0624826